

# Order-by-disorder and spiral spin-liquid in frustrated diamond-lattice antiferromagnets

DORON BERGMAN<sup>1\*</sup>, JASON ALICEA<sup>1</sup>, EMANUEL GULL<sup>2</sup>, SIMON TREBST<sup>3</sup> AND LEON BALENTS<sup>1</sup>

<sup>1</sup>Department of Physics, University of California, Santa Barbara, California 93106-9530, USA

<sup>2</sup>Theoretische Physik, Eidgenössische Technische Hochschule Zürich, CH-8093 Zürich, Switzerland

<sup>3</sup>Microsoft Research, Station Q, University of California, Santa Barbara, California 93106, USA

\*e-mail: doronber@physics.ucsb.edu

Published online: 21 May 2007; doi:10.1038/nphys622

**Frustration refers to competition between different interactions that cannot be simultaneously satisfied—a familiar feature in many magnetic solids. Strong frustration leads to highly degenerate ground states and a large suppression of ordering by fluctuations. Key challenges in frustrated magnetism include the characterization of the fluctuating spin-liquid regime and determination of the mechanism of eventual order at lower temperature. Here, we study a model of a diamond-lattice antiferromagnet appropriate for numerous spinel materials. With sufficiently strong frustration, a massive ground-state degeneracy develops amongst spirals whose propagation wavevectors reside on a continuous two-dimensional ‘spiral surface’ in momentum space. We argue that an important ordering mechanism is entropic splitting of the degenerate ground states, an elusive phenomenon called ‘order by disorder’. A broad spiral spin-liquid regime emerges at higher temperatures, where the underlying spiral surface can be directly revealed through spin correlations. We discuss the agreement between these predictions and the well-characterized spinel  $\text{MnSc}_2\text{S}_4$ .**

When microscopic interactions in a material conspire to ‘accidentally’ produce many nearly degenerate low-energy states, otherwise weak residual effects can give rise to remarkable emergent behaviour. This theme recurs throughout modern condensed-matter physics. Quintessential examples include the cuprates, with several competing orders including high- $T_c$  superconductivity, and exotic quantum (Hall) liquids in two-dimensional electron systems, arising from partial Landau-level occupation. Insulating magnets constitute a particularly abundant source of such phenomena, as in numerous cases frustration generated by the competition between different exchange interactions leads to large classical ground-state degeneracies. An important experimental signature of such degeneracies is an anomalously low ordering temperature,  $T_c$ , relative to the Curie–Weiss temperature,  $\Theta_{\text{CW}}$ ; indeed, values of the ‘frustration parameter’  $f = |\Theta_{\text{CW}}|/T_c$  larger than 5–10 are typically taken as empirical evidence of a highly frustrated magnet<sup>1</sup>. This sharp suppression of  $T_c$  opens up a broad ‘spin-liquid’ regime for temperatures  $T_c \lesssim T \lesssim |\Theta_{\text{CW}}|$ , where the system fluctuates amongst the many low-energy configurations but evades long-range order. Highly non-trivial physics can emerge here, as attested for instance in pyrochlore antiferromagnets by the experimental observation of hexagonal loop correlations in neutron scattering on the spinel  $\text{ZnCr}_2\text{O}_4$  (ref. 2), and theoretically by the establishment of ‘dipolar’ correlations<sup>3–5</sup>.

Low-temperature ordering in highly frustrated magnets often exhibits an exquisite sensitivity to degeneracy-breaking perturbations, notably dipolar interactions and minimal disorder in the spin-ice pyrochlores<sup>6</sup>, spin-lattice coupling in various spinels<sup>7</sup> and Dzyaloshinskii–Moriya interactions in  $\text{Cs}_2\text{CuCl}_4$  (ref. 8). However, the lifting of degeneracy need not require the presence of such explicit perturbations. This can be achieved, rather remarkably, by fluctuations—a process commonly referred

to as ‘order-by-disorder’<sup>9</sup>. Here, degeneracy in the free energy is lifted entropically, resulting in ordering that counter-intuitively is enhanced by increasing temperature. An analogous phenomenon occurs in quantum spin models at  $T = 0$ , where quantum fluctuations provide the degeneracy-breaking mechanism<sup>10–12</sup>. Whether or not order-by-disorder transpires depends crucially on the degree of degeneracy: for instance, it is known to occur in various face-centred-cubic (f.c.c.) antiferromagnets<sup>13,14</sup>, but not in the more severely degenerate nearest-neighbour pyrochlore antiferromagnet<sup>15,16</sup>, where instead a classical spin-liquid regime extends down to  $T = 0$ . Although these ideas have existed for decades and enjoy broad acceptance in the theoretical community, compelling experimental evidence for order-by-disorder in even one example is currently lacking.

Here, we argue that entropic effects may play a key role in the physics of insulating normal spinels, with the generic chemical formula  $\text{AB}_2\text{X}_4$ , that comprise antiferromagnets on a diamond lattice formed by magnetic, orbitally non-degenerate A sites (see Fig. 1). Numerous strongly frustrated materials in this class have been recent subjects of intensive experimental study; in particular,  $\text{CoAl}_2\text{O}_4$  and  $\text{MnSc}_2\text{S}_4$  for which  $f > 10$ –20 (refs 17,18) and  $f \approx 10$  (ref. 19), respectively, are expected to provide ideal test grounds for the physics that we describe. We introduce a simple classical model for these materials, consisting of a basic ‘parent’ hamiltonian supplemented by small corrections, that exhibits complex behaviour in accord with numerous experimental observations. Remarkably, ground states of the parent theory are (for most of its phase space) highly degenerate coplanar spirals, whose propagation wavevectors form a continuous surface in momentum space. Within our parent theory, order-by-disorder occurs with a dramatically suppressed  $T_c$  relative to  $\Theta_{\text{CW}}$ , and above  $T_c$  a ‘spiral spin-liquid’ regime emerges where the system fluctuates

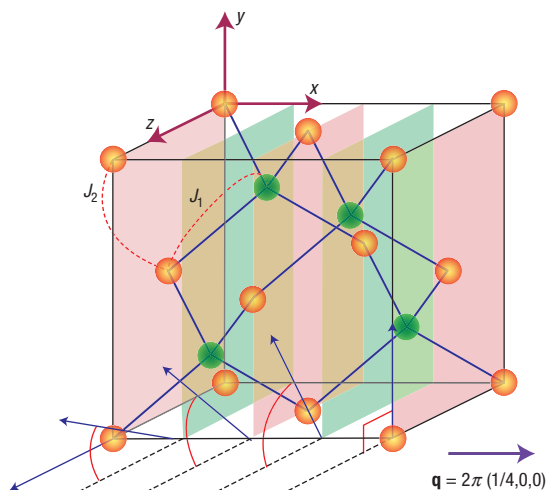


**Figure 1** Spin-spiral state on the diamond lattice. The diamond lattice, composed of two interpenetrating f.c.c. sublattices (coloured orange and green). Second-neighbour antiferromagnetic exchange,  $J_2$ , generates strong frustration, which the competition from  $J_1$  can significantly enhance. For  $J_2/J_1 > 1/8$ , this results in a large ground-state degeneracy consisting of spin spirals whose propagation wavevectors lie on a two-dimensional surface in momentum space. The blue arrows above denote the orientations of spins in the shaded planes for one such spiral with wavevector  $\mathbf{q} = 2\pi(1/4, 0, 0)$ , shown for ferromagnetic  $J_1$  for clarity.

among these degenerate spirals. Although the small corrections (which we describe) inevitably determine specific ground states at the lowest temperatures, entropy washes these out at higher temperatures, allowing the spiral spin-liquid and/or order-by-disorder physics inherent to the parent hamiltonian to become visible. This energy-entropy competition is thus manifest as an interesting multistage ordering behaviour.

Superficially, the strong frustration inherent in materials such as  $\text{MnSc}_2\text{S}_4$  seems rather puzzling. Indeed, the diamond lattice is bipartite, and accordingly a model with only nearest-neighbour spin coupling,  $J_1$ , whether ferromagnetic or antiferromagnetic, exhibits no frustration. Additional interactions must therefore be incorporated to account for the observed frustration. We first consider the simplest modification that achieves this, and assume a hamiltonian with additional second-neighbour antiferromagnetic exchange,  $J_2$ :

$$H = J_1 \sum_{\langle ij \rangle} \mathbf{S}_i \cdot \mathbf{S}_j + J_2 \sum_{\langle\langle ij \rangle\rangle} \mathbf{S}_i \cdot \mathbf{S}_j. \quad (1)$$

Here, the spins  $\mathbf{S}_i$  are modelled as classical three-component unit vectors (absorbing a factor of  $S(S+1)$  into the definition of  $J_i$ ), appropriate to the large spin values ( $S = 3/2, 5/2$ ) for these materials. Throughout, we set the lattice constant  $a = 1$  and consider  $J_2 > 0$  appropriate for antiferromagnetic exchange. Although the sign of  $J_1$  can always be changed by sending  $\mathbf{S}_i \rightarrow -\mathbf{S}_i$  on one of the two diamond sublattices, for ease of discussion we will assume antiferromagnetic  $J_1 > 0$  unless specified otherwise. Additional interactions such as further-neighbour exchange may also be present, but will be assumed small and returned to only at the end of the paper. As we will see, the parent hamiltonian, equation (1), leads to a rich theoretical picture, which we argue captures the essential physics operating in these strongly frustrated materials.

To appreciate the frustration in  $H$ , it is convenient to view the diamond lattice as being composed of two interpenetrating

f.c.c. sublattices (coloured orange and green in Fig. 1). From this perspective,  $J_1$  couples the two f.c.c. sublattices, whereas  $J_2$  couples nearest-neighbours within each f.c.c. sublattice. The f.c.c. antiferromagnet is known to be highly frustrated<sup>20</sup>, in the sense that it has a rather large frustration parameter,  $f \approx 8$  (refs 14,21–23), and hence  $J_2$  generates strong frustration, which the competition from  $J_1$  can significantly enhance. Furthermore, although further-neighbour exchanges are typically assumed to be weak, the complexity of exchange paths in such materials<sup>19,24,25</sup> suggests that  $J_1$  and  $J_2$  may indeed have comparable strengths.

We begin by discussing the zero-temperature properties of equation (1). Using the Luttinger–Tisza method<sup>26–29</sup>, exact ground states can be obtained for arbitrary  $J_2/J_1$ . The derivation is shown in Supplementary Information, Section I A. In the weakly frustrated limit with  $0 \leq J_2/J_1 \leq 1/8$ , the ground state is the Néel phase, with each spin anti-aligned with those of its nearest neighbours. For larger  $J_2$ , the simple Néel phase is supplanted by a massively degenerate set of coplanar spin spirals. As shown schematically in Fig. 1, each spiral ground state is characterized by a single wavevector,  $\mathbf{q}$ , lying on a two-dimensional ‘spiral surface’. This surface possesses a nearly spherical geometry for coupling strengths  $1/8 < J_2/J_1 < 1/4$ , and exhibits an open topology for  $J_2/J_1 > 1/4$  where it develops ‘holes’ centred around the (111) directions (see Fig. 2). In the limit  $J_2/J_1 \rightarrow \infty$ , the surface collapses into one-dimensional lines, which are known to characterize the ground states of the nearest-neighbour-coupled f.c.c. antiferromagnet<sup>20</sup>. Other systems such as the rhombohedral antiferromagnet of refs 10,30 also exhibit degenerate spirals characterized by lines in momentum space. Our model, with a spiral surface, provides an interesting intermediate case between these examples and the more highly frustrated pyrochlore antiferromagnet. Whether this degeneracy is severe enough to suppress long-range order down to zero temperature, as in the pyrochlore model, will be determined by our analysis that follows.

At small but non-zero temperature, we must consider both the local stability and the global selection amongst these ground states. The stability issue is quite delicate, as at  $T = 0$  the spins can smoothly distort from one ground state to any other at no energy cost. More formally, for any ground state at  $T = 0$  there is a fluctuation stiffness,  $\kappa_0(\mathbf{q})$ , that has an infinite number of zeros, vanishing for any  $\mathbf{q}$  on the spiral surface. The spin-wave frequencies for the associated branch of normal modes around a spiral state also vanish at these momenta, and are given by  $\omega_0^2(\mathbf{q}) = c(\mathbf{q})\kappa_0(\mathbf{q})$ , where  $c(\mathbf{q})$  is non-vanishing for  $\mathbf{q}$  on the spiral surface (see the Supplementary Information). This leads to a divergence in a naïve low-temperature expansion in small fluctuations. To illustrate, let us start from an arbitrary ground state ordered at wavevector  $\mathbf{Q}$ , with a corresponding spin configuration,  $\bar{\mathbf{S}}_i$ , and expand the hamiltonian in fluctuations  $\delta\mathbf{S}_i = \mathbf{S}_i - \bar{\mathbf{S}}_i$ . To leading order in temperature, the thermally averaged fluctuation amplitude, by equipartition, is given by

$$\langle \delta\mathbf{S}_i^2 \rangle \sim T \int \frac{d^3\mathbf{q}}{\kappa_0(\mathbf{q})} \rightarrow \infty, \quad (2)$$

which diverges owing to the infinite number of zeros in  $\kappa_0(\mathbf{q})$ . However, as only a finite number of these zeros, related to the ‘Goldstone modes’ in this model, are guaranteed by symmetry, thermal fluctuations can lift the remaining ‘accidental’ zeros, potentially stabilizing an ordered state.

This stabilization indeed occurs. Interestingly, modifications to  $\kappa_0(\mathbf{q})$  by thermal fluctuations are non-perturbative in temperature. We therefore obtain the leading corrections for  $T \ll \Theta_{\text{CW}}$  within a self-consistent treatment as described in the Supplementary

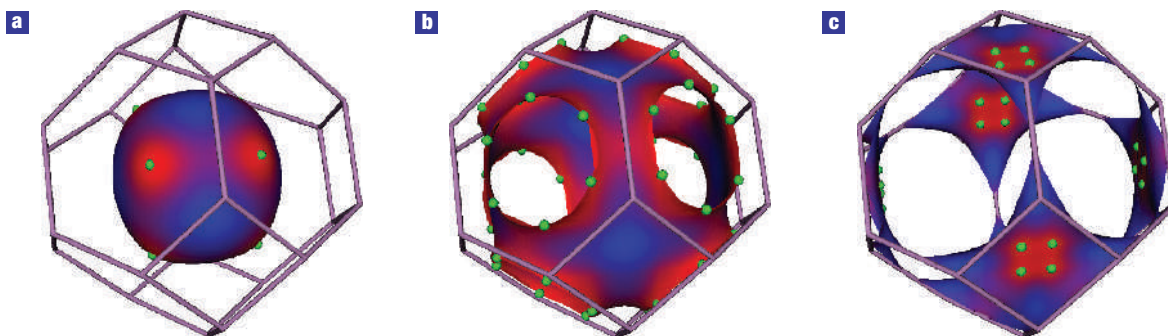


**Figure 2** Spiral surfaces. **a–c**, ‘Spiral surfaces’ comprising the degenerate spiral ground-state wavevectors for coupling strengths  $J_2/J_1$  of 0.2 (**a**), 0.4 (**b**) and 0.85 (**c**), where the last value is appropriate for  $\text{MnSc}_2\text{S}_4$ . Order-by-disorder occurs at finite temperature, as thermal fluctuations lift the degeneracy in the free energy. The surfaces are colour-coded according to the resulting low-temperature free energy at each wavevector, with high values being blue, low values being red, and green being the absolute minima.

Information. Provided  $J_1 \neq 0$ , we find that for  $\mathbf{q}$  near the spiral surface the stiffness becomes

$$\kappa_T(\mathbf{q}) = \kappa_0(\mathbf{q}) + T^{2/3} \Sigma(\mathbf{q}), \quad (3)$$

where  $\Sigma(\mathbf{q})$  is temperature independent and generically vanishes only at the spiral wavevectors  $\pm\mathbf{Q}$ , which are precisely the locations of the Goldstone modes. Thus, entropy indeed lifts the surface degeneracy, which cures the divergence in equation (2) and stabilizes long-range order. Nevertheless, the order is in a sense ‘unconventional’ in that anomalies in thermodynamic quantities appear owing to the non-analytic temperature dependence in equation (3). In particular, the classical specific heat at low temperatures scales as

$$C_v^{\text{classical}}(T) = A + BT^{1/3},$$

where  $A$  and  $B$  are constants. A crude quantum treatment, obtaining the magnon spectrum,  $\hbar\omega_0(\mathbf{q}) \sim \sqrt{\kappa_T(\mathbf{q})}$ , by quantizing the classical spin-wave modes, predicts the fractional power law,  $C_v^{\text{quantum}}(T) \sim T^{7/3}$ . This is intriguingly reminiscent of the approximately  $T^{2.5}$  behaviour observed in  $\text{CoAl}_2\text{O}_4$  (ref. 18) and related materials<sup>19</sup>.

We now address which state thermal fluctuations select. Although the energy,  $E$ , associated with each wavevector on the spiral surface is identical, their entropy,  $S$ , and hence free energy,  $F = E - TS$ , generally differ. Typically, entropy favours states with the highest density of nearby low-energy excitations. To compute the free energy at low temperatures, it suffices to retain terms in the hamiltonian that are quadratic in fluctuations about a state ordered at wavevector  $\mathbf{Q}$ . The free energy can then be computed numerically for each  $\mathbf{Q}$  on the surface. The results for select  $J_2/J_1$  are shown in Fig. 2, where the surface is coloured according to the magnitude of the free energy (blue is high, red is low and the global minima are green). As indicated in Fig. 3, the free-energy minima occur at the following locations as  $J_2/J_1$  varies: (1) along the  $(q, q, q)$  directions for  $1/8 < J_2/J_1 \leq 1/4$  as in Fig. 2a; (2) at the six wavevectors shown in Fig. 2b located around each ‘hole’ in the surface for  $1/4 < J_2/J_1 \leq 1/2$ ; (3) along the  $(q, q, 0)$  directions when  $1/2 \leq J_2/J_1 \leq 2/3$ ; and (4) at four points centred around each  $(q, 0, 0)$  direction as in Fig. 2c for larger  $J_2$ . Eventually the latter points converge precisely onto the  $(q, 0, 0)$  directions, where the nearest-neighbour f.c.c. antiferromagnet is known to order<sup>14</sup>.

Next, we turn to the evolution with increasing temperature, for which we rely on extensive Monte Carlo simulations and analytic

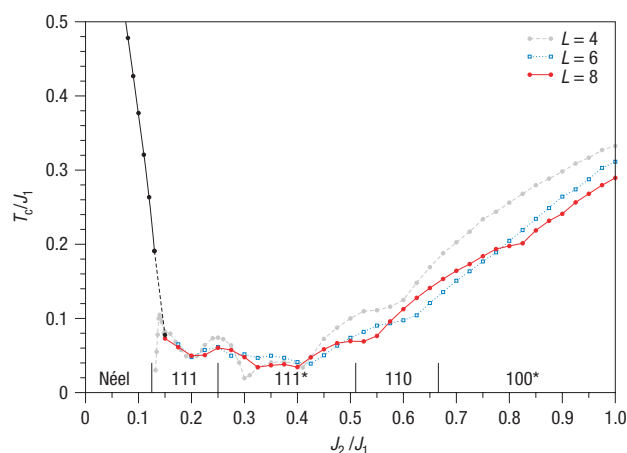


**Figure 3** Phase diagram. Numerical results for the ordering temperature,  $T_c$ , versus the coupling strength,  $J_2/J_1$ , for systems with up to  $N = 8 \times L^3 = 4,096$  spins. The ordering temperature rapidly diminishes in the Néel phase on adding  $J_2$ , and remains finite for  $J_2/J_1 > 1/8$  where the spiral surface occurs in agreement with our order-by-disorder analysis. The entropically selected ordering at low temperatures is shown along the horizontal axis; 111\* and 100\* refer respectively to the green points in Fig. 2b and c. The ‘bumpy’ modulations in  $T_c$  originate from an unusual finite size effect, namely variations in the number of momenta in the Brillouin zone that for the finite system approximate the spiral surface.

arguments. As we introduce frustration via  $J_2$ , it is natural to expect a sharply reduced transition temperature,  $T_c$ , relative to  $\Theta_{\text{CW}}$ , and this is indeed borne out in our simulations. Figure 3 shows  $T_c/J_1$  versus  $J_2/J_1$  computed numerically for systems with up to  $N = 4,096 = 8 \times 8^3$  spins. In the Néel phase, a sharp decrease in  $T_c$  is evident on increasing  $J_2$ . As an interesting aside, for  $J_2/J_1$  just above  $1/8$  two ordering transitions appear below the paramagnetic phase. This occurs due to thermal stabilization of the Néel phase slightly beyond the value of  $J_2/J_1 = 1/8$ ; the re-entrant Néel order appears below the dashed black line in Fig. 3. More interestingly,  $T_c$  clearly remains non-zero for  $J_2/J_1 > 1/8$ , in agreement with the preceding order-by-disorder analysis. Throughout this region, the transition is strongly first order.

Owing to the strong suppression of  $T_c$  when  $J_2/J_1 > 1/8$ , we can explore a broad range of the spin-liquid regime in the paramagnetic

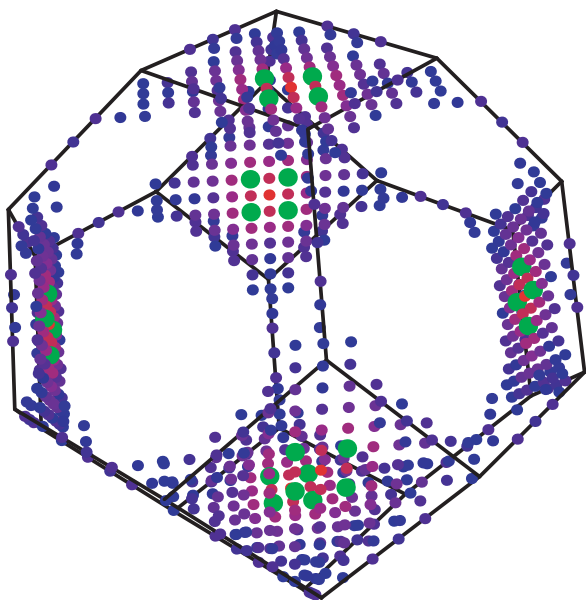


**Figure 4** Spiral surface measured from Monte Carlo simulation. Regions of high intensity in the magnetic structure factor in the paramagnetic phase just above  $T_c$ . The data were obtained numerically for a system with  $N = 8 \times 12^3 = 13,824$  spins at coupling strength  $J_2/J_1 = 0.85$  appropriate for  $\text{MnSc}_2\text{S}_4$ . As demonstrated by the remarkable similarity to Fig. 2c, the structure factor not only clearly reveals the underlying spiral surface, but also reflects the entropic corrections to the free energy along the surface.

state above  $T_c$  and below  $|\Theta_{\text{CW}}|$ . Interestingly, the spiral surface, as well as entropic free-energy corrections, can be directly probed via the spin structure factor. This is illustrated in Fig. 4, which shows the structure factor,  $S^{\text{AA}}(\mathbf{q})$ , corresponding to spin correlations on one of the two f.c.c. sublattices. (Experimentally,  $S^{\text{AA}}(\mathbf{q})$  can be obtained from the full structure factor as described in the Supplementary Information.) The data correspond to  $N = 13,824$  spins with  $J_2/J_1 = 0.85$ , relevant for  $\text{MnSc}_2\text{S}_4$  as discussed below, at a temperature just above  $T_c$ . Here, we plot only momenta contributing the highest 44% intensity (blue points have lower intensity, red higher and green corresponds to the maxima); the similarity to Fig. 2c is rather striking. The free-energy splitting manifest here persists up to  $T \approx 1.3T_c$ , whereas the surface itself remains discernible out to  $T \approx 3T_c$  (see Fig. 5). The spiral ground states evidently dominate the physics for  $T_c \lesssim T \lesssim 3T_c$ , so that this regime can be appropriately characterized as a ‘spiral spin-liquid’.

To quantify the behaviour in this regime analytically, we calculated the structure factor within the ‘spherical’ approximation, in which the unit-magnitude constraint on each spin is relaxed to  $\sum_i |\mathbf{S}_i|^2 = N$ . The classical spin liquids in Kagomé<sup>31</sup> and pyrochlore<sup>3</sup> antiferromagnets are known to be well described by this scheme. Here, we find that the structure factor is similarly peaked on the spiral surface, with a width  $\xi^{-1} \sim k_B T$  (where  $k_B$  is Boltzmann’s constant) that agrees quantitatively with the fitted value from numerics. Moreover, the complete three-dimensional structure factor data collapse onto a (known) one-dimensional curve when plotted versus the variable

$$\Lambda(\mathbf{q}) = 2\sqrt{\cos^2 \frac{q_x}{4} \cos^2 \frac{q_y}{4} \cos^2 \frac{q_z}{4} + \sin^2 \frac{q_x}{4} \sin^2 \frac{q_y}{4} \sin^2 \frac{q_z}{4}}.$$

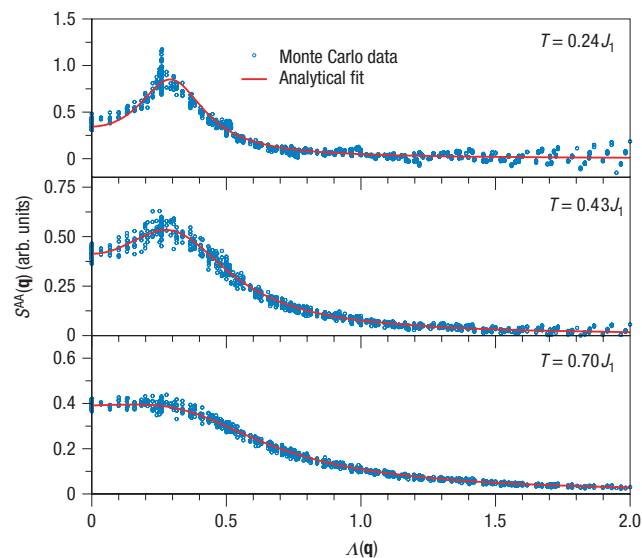


**Figure 5** Correlation function of the spiral spin-liquid. Structure factor data,  $S^{\text{AA}}(\mathbf{q})$ , versus  $\Lambda(\mathbf{q})$  in the paramagnetic phase with  $J_2/J_1 = 0.85$ , for which  $T_c \approx 0.22J_1$ . Essentially for all  $T > T_c$ , the numerical data agree quantitatively with the spherical-model predictions, with one fitting parameter corresponding to an overall scaling factor. The peaks in the upper two panels correspond to points near the spiral surface, which remains discernible up to  $T \approx 3T_c$ .

As shown in Fig. 5 for  $J_2/J_1 = 0.85$ , the numerical data conform well to this prediction, essentially throughout the paramagnetic phase except very near  $T_c$  where thermal fluctuations dramatically split the free energy along the surface. Note that the red analytical curves contain only a single fitting parameter, corresponding to an unimportant overall scaling.

Finally, we discuss implications for experiments, focusing on the well-characterized material  $\text{MnSc}_2\text{S}_4$ . Below  $T_{N1} = 2.3$  K, experiments observe long-range spiral order with wavevector  $\mathbf{Q}_{\text{exp}} \approx 2\pi(3/4, 3/4, 0)$ , coexisting with pronounced correlations with wavevector magnitude  $Q_{\text{diff}} \approx 2\pi$  that persist to well above  $T_{N1}$  (refs 25,32). A second transition occurs at  $T_{N2} = 1.9$  K, below which the latter correlations are greatly suppressed. Assuming  $\mathbf{Q}_{\text{exp}}$  lies near the spiral surface, we estimate that  $J_2/J_1 \approx 0.85$  for this material. By comparing the structure of the spiral ground state ordered at  $\mathbf{Q}_{\text{exp}}$  with the experimentally determined spin structure<sup>25</sup>, we further deduce that  $J_1$  must be ferromagnetic (that is,  $J_1 < 0$ ) in  $\text{MnSc}_2\text{S}_4$ . We can then extract the magnitudes of the exchange constants from the measured Curie–Weiss temperature,  $\Theta_{\text{CW}} \approx -22.1$  K; we obtain  $J_1 \approx -10.5$  K and  $J_2 \approx 8.75$  K. According to the numerical results of Fig. 3, the predicted ordering temperature for these parameters is  $T_c \approx 2.4$  K.

Obtaining a detailed comparison to the low-temperature experimental order requires perturbing our parent hamiltonian. Quite generally, these corrections inevitably overwhelm the entropic free-energy splittings discussed above at sufficiently low temperature, as the splittings vanish as  $T \rightarrow 0$ . Fortunately, the simplest correction—a small antiferromagnetic third-neighbour exchange,  $J_3$ —favours the observed  $(q, q, 0)$  spiral direction. The close proximity of the calculated  $T_c$  for  $J_3 = 0$  to the experimental  $T_{N1}$  suggests that  $J_3$  should indeed be small. For sufficiently small  $J_3$ , the entropic splittings will outweigh this energetic correction at higher temperatures, giving way to an intermediate phase with long-range spiral order along the entropically favoured



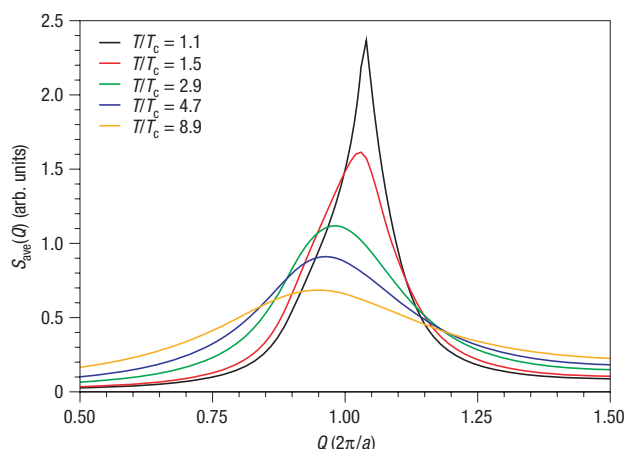


**Figure 6 Powder-averaged structure factor.** Powder-averaged structure factor in the spherical model with  $J_2 = -0.85J_1$  and  $J_3 = -J_1/20$ . The data correspond to temperatures ranging from just above  $T_c$  to several times  $T_c$ . Corrections due to  $J_3$  initially dominate the signal, but are rapidly washed out as the temperature increases, leaving the robust spiral spin-liquid correlations. The data reproduce well the diffuse scattering around  $Q_{\text{diff}} \approx 2\pi$  observed in powder neutron experiments.

(approximately)  $(q, 0, 0)$  directions. As  $J_3$  increases (but remains small), this order-by-disorder phase will be weakened and eventually removed, leaving only the more robust spiral spin-liquid correlations above  $T_c$ . The  $Q_{\text{diff}}$  scattering deduced from powder neutron experiments is consistent with weak order-by-disorder as well as our predictions for the spiral spin-liquid, and further single-crystal experiments are needed to distinguish between these scenarios. For comparison with measurements, in Fig. 6 we show the numerically powder-averaged spherical-model structure factor,  $S_{\text{ave}}(Q)$ , for  $J_3 = |J_1|/20$  at several temperatures above  $T_c$ . This reproduces well the experimental diffuse correlations near  $Q_{\text{diff}}$  as temperature smears the  $J_3$  splitting. In short, the ‘competing order’ observed at intermediate temperatures is precisely in line with theoretical expectations in our framework, and thus in our view provides convincing experimental evidence for our model’s relevance to the physics of  $\text{MnSc}_2\text{S}_4$ .

In future, many other materials are anticipated to be described by our model, from the marginally frustrated  $\text{CoRh}_2\text{O}_4$  and  $\text{MnAl}_2\text{O}_4$  with  $f \approx 1.2$  and  $f \approx 3.6$ , respectively, to the highly frustrated  $\text{CoAl}_2\text{O}_4$ . Existing measurements place a lower bound on the frustration parameter for  $\text{CoAl}_2\text{O}_4$  of around 10–20; a broad peak in the specific heat evidently pre-empt a sharp ordering transition in current samples<sup>17,18</sup>. As described in the Supplementary Information, the available low-temperature powder neutron data together with the large frustration parameter are consistent with this material residing in the region  $J_2/J_1 \approx 1/8$ , where the spiral surface begins to develop. Experiments with increased sample purity would probably provides a more direct comparison. Regarding future experiments more generally, single-crystal neutron data would be most exciting; this would lead to a much more direct and detailed comparison of theory and experiment. One could carry out an analysis similar to the one carried out for the structure factor in our Monte

Carlo simulations, as detailed in the Supplementary Information. In this way, one might directly observe the spiral surface in the spiral spin-liquid regime and perhaps find the first unambiguous experimental signatures of order-by-disorder, both of which would be truly remarkable.

Received 20 November 2006; accepted 20 April 2007; published 21 May 2007.

## References

- Ramirez, A. P. Strongly geometrically frustrated magnets. *Annu. Rev. Mater. Sci.* **24**, 453–480 (1994).
- Lee, S.-H *et al.* Emergent excitations in a geometrically frustrated magnet. *Nature* **418**, 856–858 (2002).
- Isakov, S. V., Gregor, K., Moessner, R. & Sondhi, S. L. Dipolar spin correlations in classical pyrochlore magnets. *Phys. Rev. Lett.* **93**, 167204 (2004).
- Henley, C. L. Power-law spin correlations in pyrochlore antiferromagnets. *Phys. Rev. B* **71**, 014424 (2005).
- Hermele, M., Fisher, M. P. A. & Balents, L. Pyrochlore photons: The U(1) spin liquid in a  $s = 1/2$  three-dimensional frustrated magnet. *Phys. Rev. B* **69**, 064404 (2004).
- Bramwell, S. T. & Gingras, M. J. P. Spin ice state in frustrated magnetic pyrochlore materials. *Science* **294**, 1495–1501 (2001).
- Yamashita, Y. & Ueda, K. Spin-driven Jahn–Teller distortion in a pyrochlore system. *Phys. Rev. Lett.* **85**, 4960–4963 (2000).
- Veilleux, M. Y., Chalker, J. T. & Coldea, R. Ground states of a frustrated spin-(1/2) antiferromagnet:  $\text{Cs}_2\text{CuCl}_4$  in a magnetic field. *Phys. Rev. B* **71**, 214426 (2005).
- Villain, J., Bidaux, R., Carton, J. P. & Conte, R. Order as an effect of disorder. *J. Physique* **41**, 1263–1272 (1980).
- Rastelli, E. & Tassi, A. Order produced by quantum disorder in the Heisenberg rhombohedral antiferromagnet. *J. Phys. C* **20**, L303–L306 (1987).
- Henley, C. L. Ordering due to disorder in a frustrated vector antiferromagnet. *Phys. Rev. Lett.* **62**, 2056–2059 (1989).
- Chubukov, A. Order from disorder in a kagomé antiferromagnet. *Phys. Rev. Lett.* **69**, 832–835 (1992).
- Henley, C. L. Ordering by disorder: Ground-state selection in fcc vector antiferromagnets. *J. Appl. Phys.* **61**, 3962–3964 (1987).
- Gvozdkova, M. V. & Zhitomirsky, M. E. Monte Carlo study of first-order transition in Heisenberg fcc antiferromagnet. *JETP Lett.* **81**, 236–240 (2005).
- Reimers, J. N. Absence of long-range order in a three-dimensional geometrically frustrated antiferromagnet. *Phys. Rev. B* **45**, 7287–7294 (1992).
- Moessner, R. & Chalker, J. T. Low-temperature properties of classical geometrically frustrated antiferromagnets. *Phys. Rev. B* **58**, 12049–12062 (1998).
- Tristan, N. *et al.* Geometric frustration in the cubic spinels  $\text{MAl}_2\text{O}_4$  ( $\text{M} = \text{Co}, \text{Fe}$ , and  $\text{Mn}$ ). *Phys. Rev. B* **72**, 174404 (2005).
- Suzuki, T., Nagai, H., Nohara, M. & Takagi, H. Melting of antiferromagnetic ordering in spinel oxide  $\text{CoAl}_2\text{O}_4$ . *J. Phys. Condens. Matter* **19**, 145265 (2007).
- Fritsch, V. *et al.* Spin and orbital frustration in  $\text{MnSc}_2\text{S}_4$  and  $\text{FeSc}_2\text{S}_4$ . *Phys. Rev. Lett.* **92**, 116401 (2004).
- Smart, J. S. *Effective Field Theories of Magnetism* (W. B. Saunders Company, Philadelphia, 1966).
- Diep, H. T. & Kawamura, H. First-order phase transition in the fcc Heisenberg antiferromagnet. *Phys. Rev. B* **40**, 7019–7022 (1989).
- Minor, W. & Giebultowicz, T. Studies of FCC Heisenberg antiferromagnets by Monte Carlo simulation on large spin arrays. *J. Phys. Colloq.* **49**, 1551 (1988).
- Alonso, J. L. *et al.* Monte Carlo study of O(3) antiferromagnetic models in three dimensions. *Phys. Rev. B* **53**, 2537–2545 (1996).
- Roth, W. L. Magnetic properties of normal spinels with only A–A interactions. *J. Physique* **25**, 507–515 (1964).
- Krimmel, A. *et al.* Magnetic ordering and spin excitations in the frustrated magnet  $\text{MnSc}_2\text{S}_4$ . *Phys. Rev. B* **73**, 014413 (2006).
- Lyons, D. H., Kaplan, T. A., Dwight, K. & Menyuk, N. Classical theory of the ground spin-state in cubic spinels. *Phys. Rev.* **126**, 540–555 (1962).
- Luttinger, J. M. & Tisza, L. Theory of dipole interaction in crystals. *Phys. Rev.* **70**, 954–964 (1946).
- Luttinger, J. M. A note on the ground state in antiferromagnetics. *Phys. Rev.* **81**, 1015–1018 (1951).
- Lyons, D. H. & Kaplan, T. A. Method for determining ground-state spin configurations. *Phys. Rev.* **120**, 1580–1585 (1960).
- Rastelli, E. & Tassi, A. The rhombohedral Heisenberg antiferromagnet: infinite degeneracy of the ground state and magnetic properties of solid oxygen. *J. Phys. C* **19**, L423–L428 (1986).
- Garanin, D. A. & Canals, B. Classical spin liquid: Exact solution for the infinite-component antiferromagnetic model on the kagomé lattice. *Phys. Rev. B* **59**, 443–456 (1999).
- Mucksch, M. *et al.* Multi-step magnetic ordering in frustrated thiospinel  $\text{MnSc}_2\text{S}_4$ . *J. Phys. Condens. Matter* **19**, 145262 (2007).

## Acknowledgements

We would like to acknowledge R. Shindou, Z. Wang, C. Henley and M. P. A. Fisher for illuminating discussions, as well as T. Suzuki, M. Muecksch and A. Krimmel for sharing their unpublished results. This work was supported by the Packard Foundation (D.B. and L.B.) and the National Science Foundation through grants DMR-0529399 (J.A.) and DMR04-57440 (D.B. and L.B.). Correspondence and requests for materials should be addressed to D.B. Supplementary Information accompanies this paper on [www.nature.com/naturephysics](http://www.nature.com/naturephysics).

## Competing financial interests

The authors declare no competing financial interests.

Reprints and permission information is available online at <http://npg.nature.com/reprintsandpermissions/>